Acta Geotechnica, Vol. 1, No. 2, pp. 113-126, 2007

Hypoplastic material constants for a well-graded granular material (UGM) for base and subbase layers of flexible pavements

H. A. Rondón[1], T. Wichtmann[2*], Th. Triantafyllidis[2], A. Lizcano[1]

[1] *Department of Civil and Environmental Engineering. Los Andes University, Bogotá D. C. (Colombia)*

[2] *Institute of Soil Mechanics and Rock Mechanics, University of Karlsruhe, Engler-Bunte-Ring 14, 76131 Karlsruhe (Germany)*

Abstract

This paper presents the results of the first phase of a research project dealing with the constitutive description of the behaviour of well-graded granular materials when used for base or subbase layers in flexible pavement structures (so-called "unbound granular materials", UGMs). Monotonic and cyclic loading is under consideration. The present paper concentrates on test results and the constitutive description of monotonic loading. Hypoplasticity in the version proposed by von Wolffersdorff is used as the constitutive model. Sets of material constants for typical UGM materials do not exist in the literature. The experimental determination of a set of constants according to the procedure proposed by Herle is described in this paper. In the monotonic triaxial tests specimens with a square cross-section were used. The paper presents a preliminary test series comparing triaxial results obtained with cylindrical and with prismatic specimens. Re-calculations of the element tests are also presented. The simulations show a good congruence with the experiments.

Key words: Flexible pavements; Well-graded granular material; UGM; Monotonic loading; Hypoplasticity; Material constants

1 Introduction

A pavement must be designed in such way that the cyclic loads imposed by the vehicles do not generate excessive permanent settlements (e.g. rutting). A flexible pavement usually consists of:

- a thin or low stiffness asphalt layer,
- the base and subbase layers (well-graded, so-called "unbound granular material", UGM) and
- the subgrade.

Many design procedures [2, 4, 9, 13, 19, 21, 25, 36, 37] assume that permanent deformations occur only in the subgrade. However, in flexible pavement structures all layers contribute to settlements, although the percentage of the single layers may be different. One could think that since the UGM of the base and subbase layers is compacted to a high density (usually > 95 % of Proctor density) during construction, the permanent deformations in these layers are small. However, due to the large stress amplitudes their contribution to the overall rutting cannot be neglected and should be considered in design criterions.

In most design procedures the UGM is modelled as a linear or non-linear elastic material. Thus, only the short-time performance, i.e. the amplitudes of deformation due to given load amplitudes (representing certain classes of vehicles), are considered. Therefore, many studies deal with the determination of the elastic constants of UGMs (resilient behaviour). In comparison to the resilient behaviour, the long-time performance, i.e. the permanent (residual, plastic) deformations in UGMs due to cyclic loading were studied less intensively (see e.g. [1, 5, 12, 26, 29, 40, 43, 44]) and most of these studies use unrealistic stress paths (i.e. triaxial tests with a constant confining pressure were performed). Some equations for the prediction of permanent deformations in UGM layers of flexible pavements can be found in [1, 26, 38]. A respective literature review will be given in a future paper together with the

*Corresponding author. Tel.: + 49-721-6082235; fax: +49-721-696096; *e-mail address:* torsten.wichtmann@ibf.uka.de

results of our cyclic laboratory tests.

Since millions of load cycles have to be considered special calculation strategies for the permanent deformations are indispensable [32]. The group of Los Andes University intends to extend the Wolffersdorff hypoplastic model [41] (Section 2.1) by a variable N (number of cycles) to predict the permanent deformations of UGMs for a given bunch of N cycles of a constant amplitude. The stiffness tensor L will be modified to change with N. This modification will be explained in detail in a future paper. Analytical equations for the settlement $s(N, \ldots)$ in the UGM will be developed based on this modified hypoplastic model.

The group of University of Karlsruhe will prove the applicability of their accumulation model [35, 45] for non-cohesive soils to pre-compacted UGMs. A vertically pre-compacted UGM sample is likely to behave differently under cyclic loading in comparison to a sand sample prepared by pluviation. Using the finite element (FE) method for a prediction of residual settlements only few cycles are calculated implicitly with many strain increments (using the Wolffersdorff hypoplastic model extended by the "intergranular strain", Niemunis & Herle [34]) and the permanent deformations due to larger packages of cycles between are predicted directly (explicitly) by the accumulation model.

Irrespective of the intended calculation strategy both groups need the material constants of the Wolffersdorff hypoplastic model for a typical UGM. For this purpose a well-graded grain size distribution curve (mean grain size $d_{50} = 6.3$ mm, coefficient of uniformity $C_u = d_{60}/d_{10} = 100$) was mixed (Section 4).

A set of hypoplastic constants for such a high value of C_u is not known to the authors. Based on tests on sands and gravels with 0.16 mm $\leq d_{50} \leq$ 2.0 mm and $1.4 \leq C_u \leq 7.2$, Herle [16] and Herle & Gudehus [18] developed correlations of the hypoplastic constants h_s and n with d_{50} and C_u:

$$h_s[\text{MPa}] = 542.5 \cdot 10^{2.525(d_{50}/d_0)/\sqrt{C_u}} \quad \text{and} \qquad (1)$$

$$n = 0.366 - 0.0341\, C_u/(d_{50}/d_0)^{0.33} \qquad (2)$$

with the reference grain size $d_0 = 1$ mm. The d_{50}- and C_u-values of the material used for the present study lie outside the range of applicability of Eqs. (1) and (2). An extrapolation to UGM materials seems not possible since for the present material, Eq. (2) delivers a negative n-value (n = -1.49, h_s = 21 MPa).

In Section 5 it is reported on laboratory tests which were performed in order to derive the hypoplastic constants according to the procedure proposed by Herle [16] (Section 2.2). The constants of the "intergranular strain" are not discussed in the present paper.

In the monotonic triaxial tests for the determination of the constant α specimens with a square cross section were used. Section 3 explains the reasons and presents a preliminary series of monotonic triaxial tests in which different specimen geometries (circular and square cross section, different heights) were compared. It is demonstrated, that cylindrical and prismatic specimens deliver similar test results.

Finally, Section 6 presents re-calculations of the laboratory tests with an element test program.

2 Hypoplasticity

Hypoplastic constitutive models (e.g. Kolymbas [23]) were developed as an alternative to elasto-plastic models. They describe the mechanical behaviour of "simple grain skeletons" (Herle [16]) phenomenologically. Hypoplastic models are incrementally non-linear, rate-independent, path-dependent and dissipative. In contrast to elasto-plasticity a splitting of the strain rate in an elastic and a plastic portion is not necessary. Furthermore, there is no need to define a yield surface explicitly because it follows from the constitutive equations. The relatively simple implementation of hypoplastic models may be seen as another advantage.

2.1 Hypoplastic model proposed by von Wolffersdorff [41]

In the following, the symbol $\cdot$ denotes multiplication with one dummy index (single contraction), e.g. $\mathbf{A} \cdot \mathbf{B} = A_{ik}B_{kj}$. A multiplication with two dummy indices (double contraction) is denoted with a colon, e.g. $\mathbf{A} : \mathbf{B} = A_{ij}B_{ij}$. Dyadic multiplication is written without $\otimes$, i.e. $\mathbf{AB} = A_{ij}B_{kl}$. $\sqcup^*$ is the deviatoric part of $\sqcup$ and $\| \sqcup \|$ denotes Euclidian normalization.

The general form of the hypoplastic model may be written as:

$$\mathring{\mathbf{T}} = \mathsf{L} : \mathbf{D} + f_d\, \mathbf{N}\, \|\mathbf{D}\| \qquad (3)$$

Therein $\mathring{\mathbf{T}}$ is the objective Jaumann stress rate and $\mathbf{D}$ is the strain rate. L and $\mathbf{N}$ are the fourth-order linear and the second-order nonlinear stiffness tensor. For sand, they can be calculated from (von Wolffersdorff [41]):

$$\mathsf{L} = f_b\, f_e\, \frac{1}{\hat{\mathbf{T}} : \hat{\mathbf{T}}} \left(F^2\, \mathsf{I} + a^2\, \hat{\mathbf{T}}\hat{\mathbf{T}} \right) \qquad (4)$$

$$\mathbf{N} = f_b\, f_e\, \frac{F\, a}{\hat{\mathbf{T}} : \hat{\mathbf{T}}} \left(\hat{\mathbf{T}} + \hat{\mathbf{T}}^* \right) \qquad (5)$$

Therein $\hat{\mathbf{T}} = \mathbf{T}/\mathrm{tr}\,\mathbf{T}$ is a dimensionless stress and $I_{ijkl} = 0.5(\delta_{ik}\delta_{jl} + \delta_{il}\delta_{jk})$ is an identity tensor. The

parameters a and F in Equations (4) and (5) describe the failure criterion of Matusoka & Nakai [28] in the deviatoric plane:

$$a = \frac{\sqrt{3}\ (3-\sin\varphi_c)}{2\ \sqrt{2}\ \sin\varphi_c} \tag{6}$$

$$F = \sqrt{\frac{\tan^2\psi}{8} + \frac{2-\tan^2\psi}{2+\sqrt{2}\ \tan\psi\ \cos(3\theta)}} - \frac{\tan\psi}{2\ \sqrt{2}} \tag{7}$$

$$\tan\psi = \sqrt{3}\ \|\hat{\mathbf{T}}^*\| \tag{8}$$

$$\cos(3\theta) = -\sqrt{6}\ \mathrm{tr}\left(\hat{\mathbf{T}}^*\cdot\hat{\mathbf{T}}^*\cdot\hat{\mathbf{T}}^*\right) / \left[\hat{\mathbf{T}}^* : \hat{\mathbf{T}}^*\right]^{\frac{3}{2}} \tag{9}$$

φ_c is the critical friction angle. The angles ψ and θ describe the position of $\mathbf{T}$ in the stress space. The factors f_d, f_e and f_b consider the influence of pressure (barotropy) and density (pyknotropy) on stiffness:

$$f_d = r_e^\alpha = \left(\frac{e-e_d}{e_c-e_d}\right)^\alpha \tag{10}$$

$$f_e = \left(\frac{e_c}{e}\right)^\beta \tag{11}$$

$$f_b = \left(\frac{e_{i0}}{e_{c0}}\right)^\beta \frac{h_s}{n}\frac{1+e_i}{e_i}\left(\frac{3p}{h_s}\right)^{1-n} \cdot \cdot\left[3+a^2-a\ \sqrt{3}\ \left(\frac{e_{i0}-e_{d0}}{e_{c0}-e_{d0}}\right)^\alpha\right]^{-1} \tag{12}$$

Therein α, β, h_s (granular hardness) and n are material constants. The void ratios e_d, e_c and e_i correspond to the densest, the critical and the loosest possible state. With increasing mean pressure p they decrease affine to each other according to Equation (13) after Bauer [6]:

$$\frac{e_i}{e_{i0}} = \frac{e_c}{e_{c0}} = \frac{e_d}{e_{d0}} = \exp\left[-\left(\frac{3p}{h_s}\right)^n\right] \tag{13}$$

In Equation (13) the index "0" in e_{i0}, e_{c0} and e_{d0} corresponds to the stress-free state ($p = 0$).

Niemunis [33] suggests to write Eq. (3) in an alternative form:

$$\mathring{\mathbf{T}} = \mathsf{L} : (\mathbf{D} - f_d\ Y\ \mathbf{m}\ \|\mathbf{D}\|) \tag{14}$$

with the degree of non-linearity $Y = \|\mathsf{L}^{-1} : \mathbf{N}\|$ and the direction of flow $\mathbf{m} = -(\mathsf{L}^{-1} : \mathbf{N})/\|\mathsf{L}^{-1} : \mathbf{N}\|$. The relationship between Y and the stress obliquity $\eta = q/p$ with $p = -(T_1 + 2T_3)/3$ and $q = -(T_1 - T_3)$ was also given by Niemunis (Eq. (4.167) in [33]):

$$Y = a\frac{\sqrt{729F^4 + 18(a^4 + 6a^2F^2 + 36F^4)\eta^2 + 4a^4\eta^4}}{\sqrt{3}[9F(a^2+3F^2) + 2a^2F\eta^2]} \tag{15}$$

2.2 Procedure for the determination of the material constants after Herle [16]

Eight material constants φ_c, h_s, n, e_{d0}, e_{c0}, e_{i0}, α and β have to be determined. The procedure has been proposed by Herle [16]:

- The critical friction angle φ_c can be determined from undrained triaxial tests or from cone pluviation tests. In the cone pluviation test, φ_c is the inclination of the cone.

- The granular hardness h_s and the exponent n describe the decrease of the void ratios e_i, e_c, e_d and e with increasing mean pressure p (Eq. (13)). The constants may be obtained from tests with a proportional compression, i.e. a compression with a linear path of deformation starting from the stress-free state. An isotropic or an oedometric compression test are suitable. Eq. (13) is fitted to the measured curves $e(p)$. Ideally, the initial void ratio of the tests should be chosen in the range $e_{c0} \le e_0 \le e_{i0}$. However, $e_0 = e_{\max}$ is thought to be a satisfactory initial state (Herle [16]).

- According to Herle [16], the void ratios for asymptotic states at $p = 0$ can be estimated from $e_{i0} \approx 1.15\ e_{\max}$, $e_{c0} \approx e_{\max}$ and $e_{d0} \approx e_{\min}$.

- The constant α controls the influence of density on the peak friction angle φ_P. In order to determine α, tests with triaxial compression may be performed on initially dense specimens. From the stress ratio $K_P = T_1/T_3$ at peak of the curves $q(\varepsilon_1)$ and with the corresponding void ratios e, e_c and e_d the constant α can be calculated:

$$\alpha = \frac{\ln\left[6\frac{(K_P+2)^2 + a^2K_P(K_P-1-\tan\nu_p)}{a(5K_P-2)(K_P+2)\sqrt{4+2(1+\tan\nu_P)^2}}\right]}{\ln r_e} \tag{16}$$

with a from Eq. (6), the pressure-referenced relative density r_e according to Eq. (10) and

$$\tan\nu_P = 2\frac{(K_P-4) + AK_P(5K_P-2)}{(5K_P-2)(1+2A)} - 1 \tag{17}$$

$$A = \frac{a^2}{(K_P+2)^2}\left[1 - \frac{K_P(4-K_P)}{5K_P-2}\right] \tag{18}$$

These equations may be derived by writing Eq. (3) for triaxial compression and considering that the stress rate vanishes at peak, i.e. setting $\dot{T}_1 = \dot{T}_2 = \dot{T}_3 = 0$.

An alternative procedure may be derived from Eq. (14). In order to obtain $\overset{\circ}{\mathbf{T}} = \mathbf{0}$, the condition $f_d Y = 1$ must be fulfilled. This leads to

$$\alpha = \frac{\ln(1/Y)}{\ln(r_e)} \,. \tag{19}$$

For triaxial compression, $F = 1$ holds and Eq. (15) simplifies towards

$$Y = a\frac{\sqrt{729 + 18(a^4 + 6a^2 + 36)\eta^2 + 4a^4\eta^4}}{\sqrt{3}[9(a^2 + 3) + 2a^2\eta^2]} \tag{20}$$

The constant α may be obtained from Eqs. (19) and (20) with triples (η_P, p_P, e_P) of stress ratio, mean pressure and void ratio at the peak of the curves $q(\varepsilon_1)$. Eq. (19) is equivalent to (but in the opinion of the authors slightly easier than) Eq. (16). The pressure p enters Eqs. (16) and (19) via e_d and e_c calculated from e_{d0} and e_{c0} using Eq. (13).

- The constant β effects an increase of the stress rate $\overset{\circ}{\mathbf{T}}$ with increasing density at $\mathbf{D}$ = constant. It can be obtained from oedometric tests on specimens with different initial densities (e.g. the tests on loose sand for h_s and n can be supplemented by tests on dense sand). For a certain pressure p the void ratio e and the constrained modulus $E_s = \Delta T_1/\Delta\epsilon_1$ are determined. T_1 is the axial stress corresponding to p and ϵ_1 is the logarithmic axial strain. If the two different densities are denoted with $\sqcup_I$ and $\sqcup_{II}$, the constant β is calculated from:

$$\beta = \frac{\ln\left(\frac{E_{sII}}{E_{sI}} \; \frac{m_I - n_I \; f_{dI}}{m_{II} - n_{II} \; f_{dII}}\right)}{\ln\left(\frac{e_I}{e_{II}}\right)} \quad \text{with} \tag{21}$$

$$m = \frac{(1 + 2K_0)^2 + a^2}{1 + 2{K_0}^2} \quad \text{and} \tag{22}$$

$$n = \frac{a\,(5 - 2K_0)(1 + 2K_0)}{3(1 + 2{K_0}^2)} \,. \tag{23}$$

(be aware that equations $m = (2 + K_0)^2 + a^2$ and $n = a(2+K_0)(5-2K_0)/3$ given below Eq. (4.28) in [16] are erroneous). These equations are obtained by reducing Eq. (3) for the oedometric case ($D_2 = D_3 = 0$) and evaluating $E_s = \dot{T}_1/D_1$. If the lateral stress is not measured the coefficient $K_0 = T_3/T_1$ can be estimated from the Jaky formula $K_0 = 1 - \sin\varphi_P$.

In the Appendix several sets of material constants that were published in the literature are summarized. An UGM-like material was not tested yet.

3 Preliminary tests: Comparison of cylindrical and prismatic triaxial specimens

In the monotonic triaxial tests for the determination of the constant α specimens with a square cross section (lateral dimensions 8.7 × 8.7 cm, height h = 18 cm) were used for the following reason. The same equipment (triaxial cell, end plates, moulds, membranes) was intended to be used for the *monotonic* and the *cyclic* triaxial tests. In some of the cyclic tests also the lateral stress T_3 was cyclically varied. In such case the amplitude of volume changes measured via the pore water is falsified by membrane penetration effects (e.g. Nicholson [31]). Local measurements of lateral deformations are indispensable to obtain a correct information about the strain loop. The local measurement of lateral deformations has been realized by using LDTs, i.e. bending strips of phosphor bronze applied with strain gauges (a method extensively used by Tatsuoka and his co-workers, the technique is described e.g. by Goto et al. [14] and Hoque et al. [20]). The application of LDTs for the measurement of lateral deformations demands a square cross section. Since the LDTs were applied only for the cyclic tests they are not discussed in detail here.

Specimens with a square cross section are being used for triaxial tests since the middle of the 1990s. They were employed to use lateral LDTs first by Hoque et al. [20] for sand, by Hayano et al. [15] for sedimentary soft rock, by Jiang et al. [22] and Anh Dan et al. [3] for well-graded gravel and by Kongsukprasert et al. [24] for cement-mixed sands (after Nawir et al. [30]). Despite its extensive use (mainly in Japanese laboratories) specimens with a square cross section are sometimes set into question because an inhomogeneous deformation is expected. Surprisingly, experimental studies comparing a circular and a square cross section can hardly be found in the literature. Thus, prior to the tests on the UGM material, we have compared results of monotonic triaxial tests with specimens with a circular and a square cross section, respectively.

The preliminary tests were performed on a medium coarse quartz sand (and not on UGM) since for sands moulds for the preparation of cylindrical and prismatic specimens were already available (for UGM a special steel mould had to be manufactured in order to prepare specimens with a proctor hammer, Section 5). The used sand has a uniform grain size distribution curve (mean grain size $d_{50} = 0.55$ mm, uniformity index $C_u = 1.8$) and a sub-angular grain shape. The specimens were prepared medium dense (I_{D0} = 0.55 - 0.58) in the first four tests and dense (I_{D0} = 0.95 - 0.99) in the three other ones (relative density is expressed by the

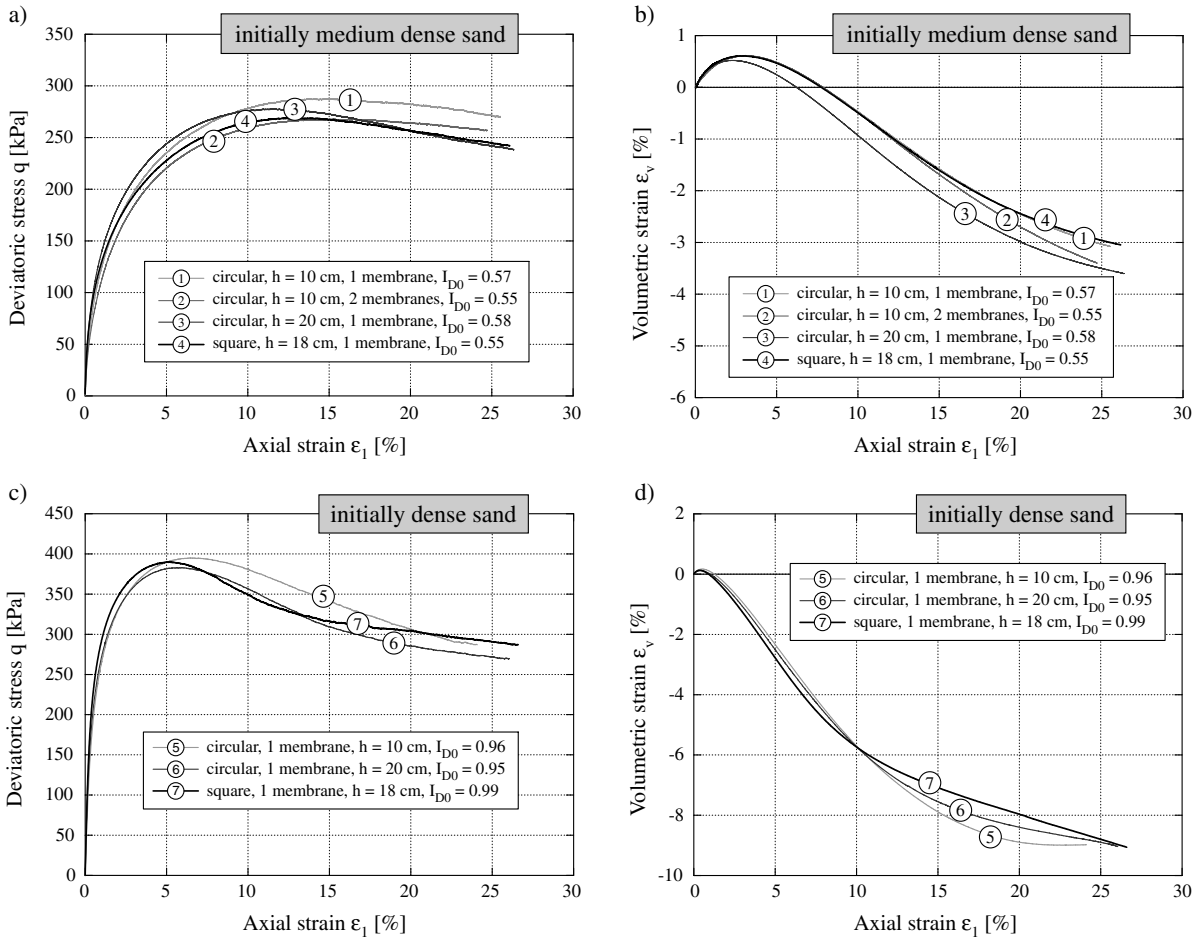

Figure 1: *Comparison of photos taken at different values of ε_1 during the monotonic triaxial tests with different specimen geometries*

index $I_D = (e_{\max} - e)/(e_{\max} - e_{\min})$ and index $\sqcup_0$ denotes the initial value). For each of these two densities, a cylindrical specimen with diameter $d = 10$ cm and height $h = 10$ cm ($h/d = 1$), a cylindrical specimen with $d = 10$ cm and $h = 20$ cm ($h/d = 2$) and a prismatic specimen with $a \times b \times h = 8.7 \times 8.7 \times 18.0$ cm ($h/a = 2.1$) were compared. Enlarged end plates were used for all specimen geometries. The end plates were lubricated with silicon grease and a thin membrane (thickness 0.4 mm) was placed on the grease layer. A good lubrication is especially important for the short specimens ($h/d = 1$). In order to study if multiple layers of silicon grease and membranes are beneficial, Test No. 2 was performed with two such layers. The lateral effective stress was $\sigma'_3 = 100$ kPa in all tests. The short specimens ($h/d = 1$) were sheared with displacement rates $\dot{u} = 0.05$ mm/min (medium dense specimens) or 0.1 mm/min (dense), respectively, and the long ones ($h/d > 2$) with $\dot{u} = 0.1$ mm/min (medium dense) or 0.2 mm/min (dense). Thus $\dot{\varepsilon_1} \approx 0.05$ %/min or 0.1 %/min holds for all tests.

Photos of the specimens at $\varepsilon_1 = 0$ %, 10 % and 20 % are given in Fig. 1. As already observed by Bishop & Green [7] cylindrical specimens with $h/d = 1$ failed by expanding at the base ("elephant foot"). Bishop & Green [7] reported that a rotation of the specimen by 180° prior to shearing lead to an expansion of the samples across the top plate. Thus, the lateral deformation of such short samples seems to depend on the gravity acting during preparation and not during shearing. Cylindrical samples with $h/d = 2$ barrelled (Fig. 1). According to Bishop & Green [7] this occurs independently of the end restraint, i.e. it does not matter if the end plates are lubricated or not. The "elephant foot" or the bulging became more pronounced with increasing initial density of the specimen (Fig. 1). Interestingly, in the case of the prismatic specimens bulging occurred for medium dense sand and an expansion at the base was observed for the dense sand. Shear zones became visible only for the dense and long specimens, irrespectively of the shape of the specimen cross section.

The curves $q(\varepsilon_1)$ and $\varepsilon_v(\varepsilon_1)$ of deviatoric stress or

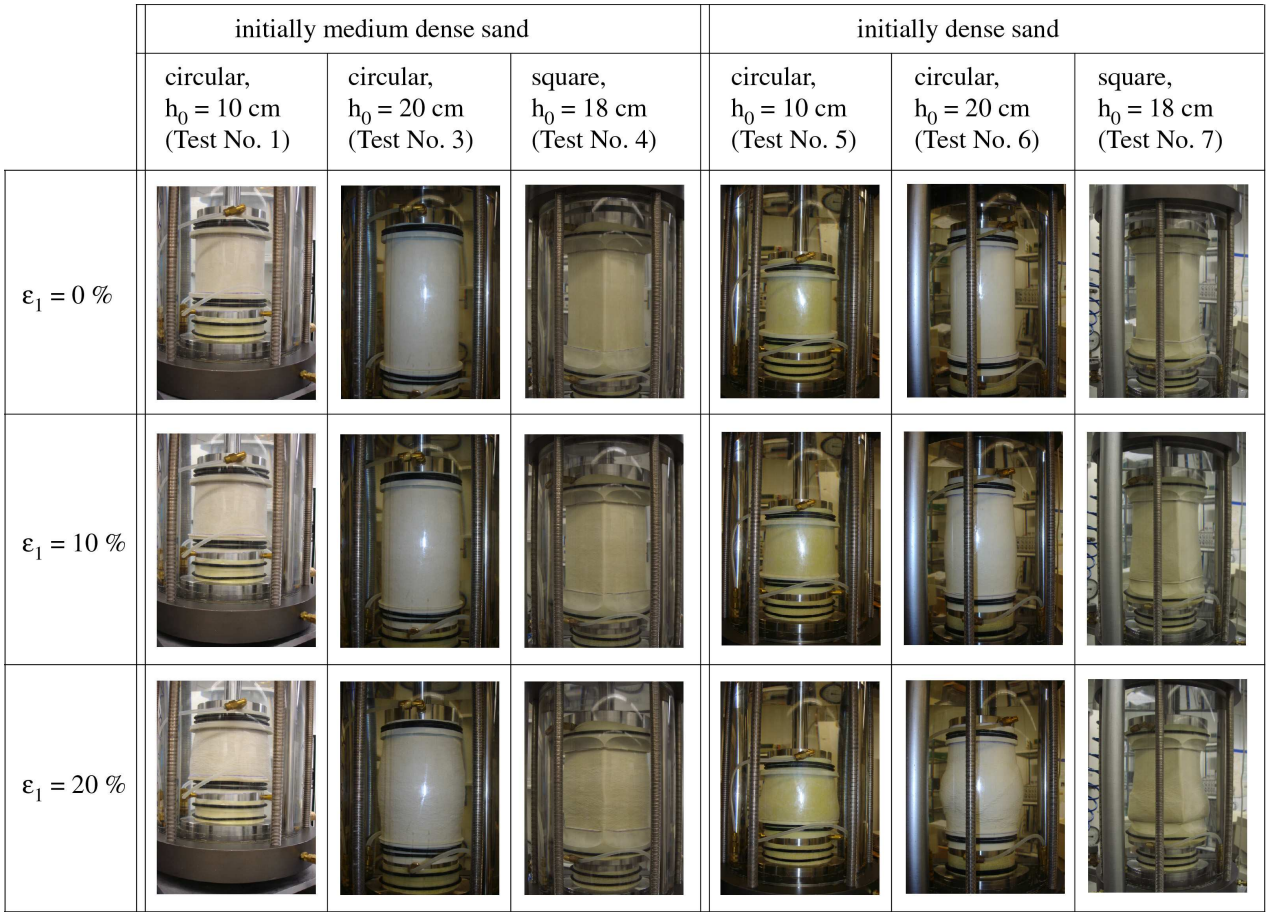

Figure 2: *Comparison of curves $q(\varepsilon_1)$ and $\varepsilon_v(\varepsilon_1)$ from monotonic triaxial tests on a medium dense sand with different specimen geometries*

volumetric strain versus axial strain are plotted in Fig. 2. The axial stress was calculated with the cross sectional area $A = V/h$ with the actual volume V and the actual height h. In comparison to the long cylindrical specimens, the short cylindrical specimens reach the peak deviatoric stress at a larger value of ε_1 and the drop of the curve $q(\varepsilon_1)$ behind the peak is less pronounced (at least for the medium dense sand). In particular for the high initial density, the curves for the specimen with the square cross section ($h/d = 2.1$) run similar to the curves for the long cylindrical sample ($h/d = 2$).

The peak friction angles φ_P are plotted versus the void ratio at peak e_P in Fig. 3. The values φ_P for the short cylindrical specimens with one lubrication layer lie approx. 1° higher than for the long cylindrical samples. The use of two lubrication layers instead of one seems to reduce φ_P, i.e. the φ_P-values come closer to the data obtained for the long cylindrical specimens. The prismatic specimens have only slightly lower φ_P-values than the long cylindrical samples.

From these preliminary tests it may be concluded

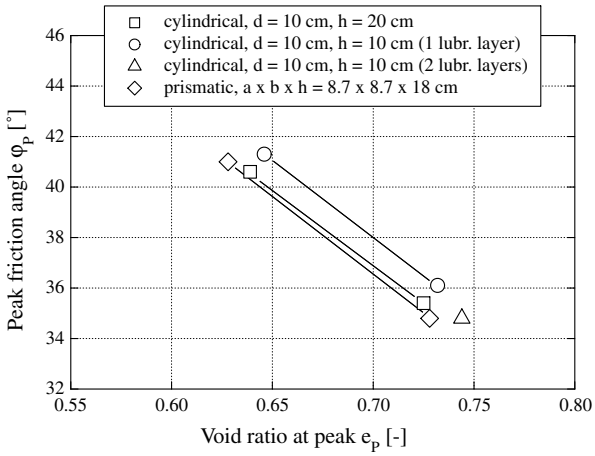

Figure 3: *Peak friction angle φ_P as a function of void ratio at peak e_P for different specimen geometries*

that circular and prismatic specimens deliver similar test results, i.e. the shape of the cross-section of a sample has only a minor effect. This was also confirmed for tests with cyclic loading as will be presented in a future

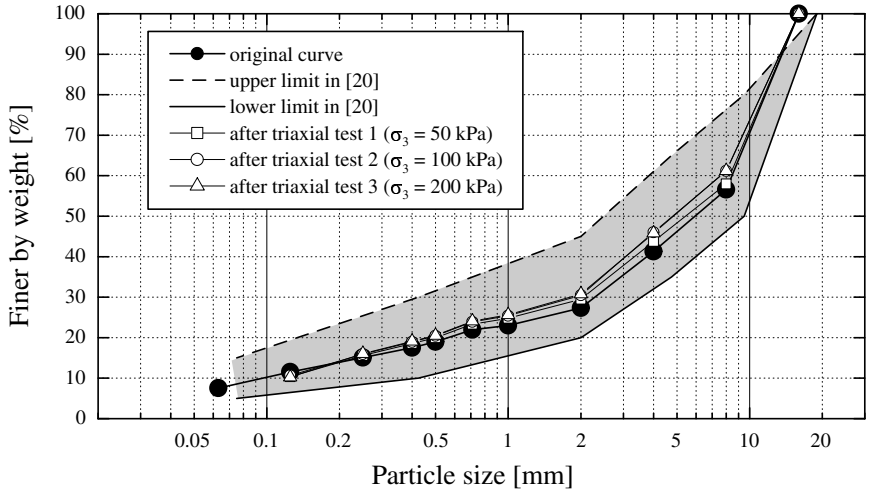

Figure 4: *Grain size distribution curve of the UGM (denoted as "original") compared to the limits of Colombian Specification [13]. Curves obtained after the monotonic triaxial tests are also given (addressed in Section 5).*

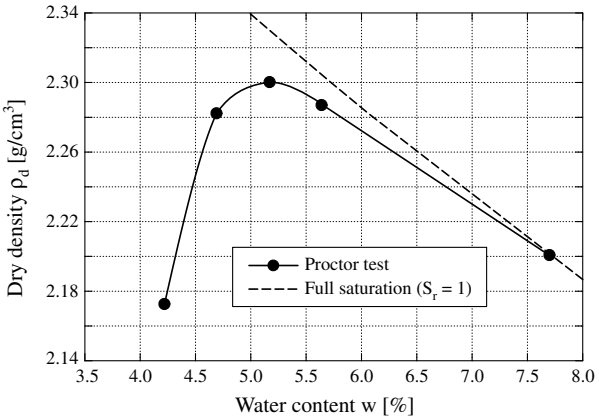

Figure 5: *Modified proctor test*

paper. Thus, the use of specimens with a square cross-section does not imply any disadvantage in connection with the determination of the hypoplastic constant α.

4 Tested Unbound Granular Material

The grain size distribution curve (Fig. 4) used in the tests is in accordance with the Colombian Specification [13] for base layer construction in flexible pavements except for the maximum grain size. It was reduced to $d_{\max} = 16$ mm in order to not fall below a ratio $a/d_{\max}$ of 5 with $a \times b$ being the dimensions of the specimen cross section in the triaxial tests. The mean grain diameter is $d_{50} = 6.3$ mm and the coefficient of uniformity is $C_u = d_{60}/d_{10} = 100$. The curve was mixed from different gradations of a quartz sand with subangular grain shape. For the fine particles a quartz meal was used. The maximum density according to German Standard Code DIN 18126 is $\varrho_{d,\max} = 2.163$ g/cm^3 (determined with a shaking table) and the minimum one is $\varrho_{d,\min} = 1.835$ g/cm^3. These values correspond to $e_{\min} = 0.225$ and $e_{\max} = 0.444$. A value $\varrho_s = 2.65$ g/cm^3 was obtained for the specific weight using a pyknometer. Fig. 5 presents the results of a Proctor test with modified energy ($E = 2700$ kNm/m^2, weight $\times$ falling height). The maximum dry density is $\varrho_{Pr} = 2.30$ g/cm^3 and the optimum water content is $w_{\text{opt}} = 5.2$ %.

5 Determination of hypoplastic material constants

The critical friction angle $\varphi_c = 38.0°$ was determined as the inclination of a pluviated cone (height approx. 12 cm). Segregation effects on φ_c can be neglected [17].

The granulate hardness h_s and the exponent n were determined from the curves $e(p)$ from four oedometric compression tests on dry, initially loose material (relative density index $I_{D0} = 0.01$ - 0.10). For a better reproducibility of the tests large specimen dimensions (diameter 28 cm, height 8 cm) were chosen. The test device is presented in Fig. 6. Specimens were prepared by pouring dry sand with a spoon. The measured curves $e(p)$ are given in Fig. 7 (upper four curves). The lateral stress was estimated as $T_3 = K_0 T_1$ with $K_0 = 1 - \sin(\varphi_c)$ and the mean pressure was calculated from $p = -(T_1 + 2T_3)/3$. Eq. (13) was fitted to each curve $e(p)$ resulting in the constants h_s and n as summarized in Table 1. Mean values $h_s = 97$ MPa and $n = 0.24$ were set into approach.

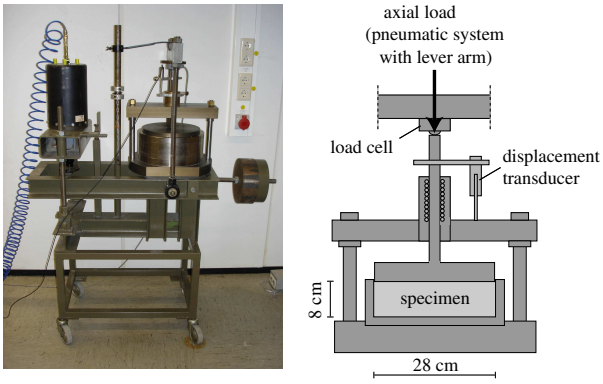

Figure 6: *Device for oedometric compression of large specimens (d = 28 cm, h = 8 cm)*

Test No.	1	2	3	4	Mean
I_{D0}	0.10	0.01	0.06	0.09	
e_{B0}	0.456	0.484	0.474	0.450	0.466
h_s [MPa]	104	116	83	86	97
n	0.247	0.221	0.228	0.275	0.24

Table 1: Summary of constants h_s and n determined from four oedometric compression tests (e_{B0} is the extrapolated void ratio at zero pressure)

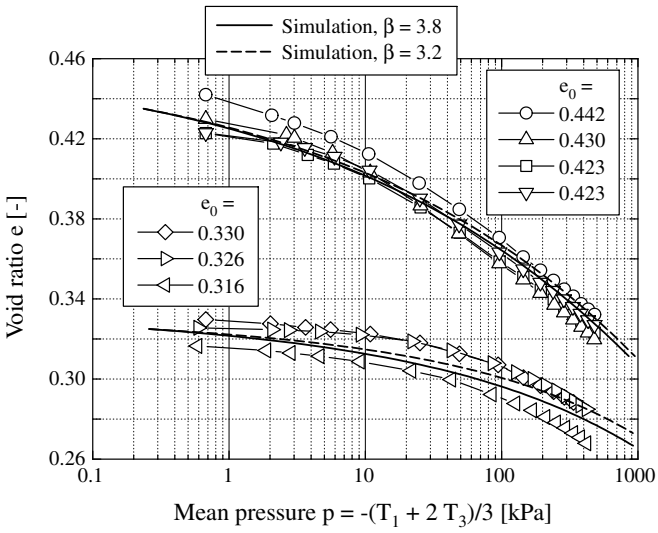

Figure 7: *Oedometric compression tests on loose and medium dense specimens (experiment and simulation, e_0 is the void ratio after sample preparation at $p \approx 0.6$ kPa)*

The limit void ratios at zero pressure were estimated from the relations $e_{d0} \approx e_{\min}$, $e_{c0} \approx e_{\max}$ and $e_{i0} \approx 1.15 e_{\max}$ (for well-graded soils) as proposed by Herle [16] with $e_{\min} = 0.225$ and $e_{\max} = 0.444$ being the minimum and maximum void ratios according to DIN 18126.

For the determination of the constant α three monotonic triaxial tests on specimens with large initial densities (I_{D0} = 1.06 - 1.13, dry density > 95% of ϱ_{Pr}) were performed. The effective lateral stresses were T_3 = -50, -100 and -200 kPa, respectively.

For the laborious specimen preparation a steel mould consisting of four plates was fixed to the bottom end plate of the triaxial cell (Fig. 8a). The specimen preparation was performed outside the triaxial cell in order to save the load cell which in the used triaxial devices (a scheme is given in Fig. 9) is located below the bottom end plate. Specimens were prepared by tamping in $n = 6$ layers each with a thickness of 3 cm. The material was in the moist condition (water content $w = w_{\text{opt}} = 5.2\%$). A miniature proctor hammer (Fig. 8b) was used. Its fall weight ($m = 1$ kg, i.e. $W = 10$ N) was dropped from a height of $H = 20$ cm and $N = 250$ blows were applied to each layer. An energy per volume (total volume of a specimen $V = 1362$ cm^3) in the order of magnitude of

$$E = \frac{N\, n\, W\, H}{V} \approx 2200 \text{ kNm/m}^3 \qquad (24)$$

was induced into a specimen. It was chosen lower than the energy used in the modified Proctor test in order to reach densities slightly lower than the modified Proctor density (95 - 97 % of ϱ_{Pr}), i.e. densities that are typical for UGMs in situ.

After tamping of the specimen the bottom end plate with the specimen was placed into the triaxial cell and the steel mould was removed (Figs. 8c,d). The specimen stands due to capillary pressure. Afterwards the membrane (diameter 110 mm, thickness 0.6 mm) was placed using a stretcher with square cross section (Fig. 5e). The specimen end plates have a special shape at the transition from the square to the round cross section. The round cross section is necessary to enable a proper sealing of the membrane by O-rings. Fig. 8f presents a specimen after the top plate was placed, the membrane was sealed, the triaxial cell was mounted and filled with water and the cell pressure was applied. Finally, the specimens were saturated with de-aired water.

Fig. 10 shows photos taken at different values of ε_1 during a test. Up to the peak the deformation is quite homogeneous but with continued shearing the upper part of the specimen expands. This is in contrast to the tests on dense sand (Section 3) where the specimen

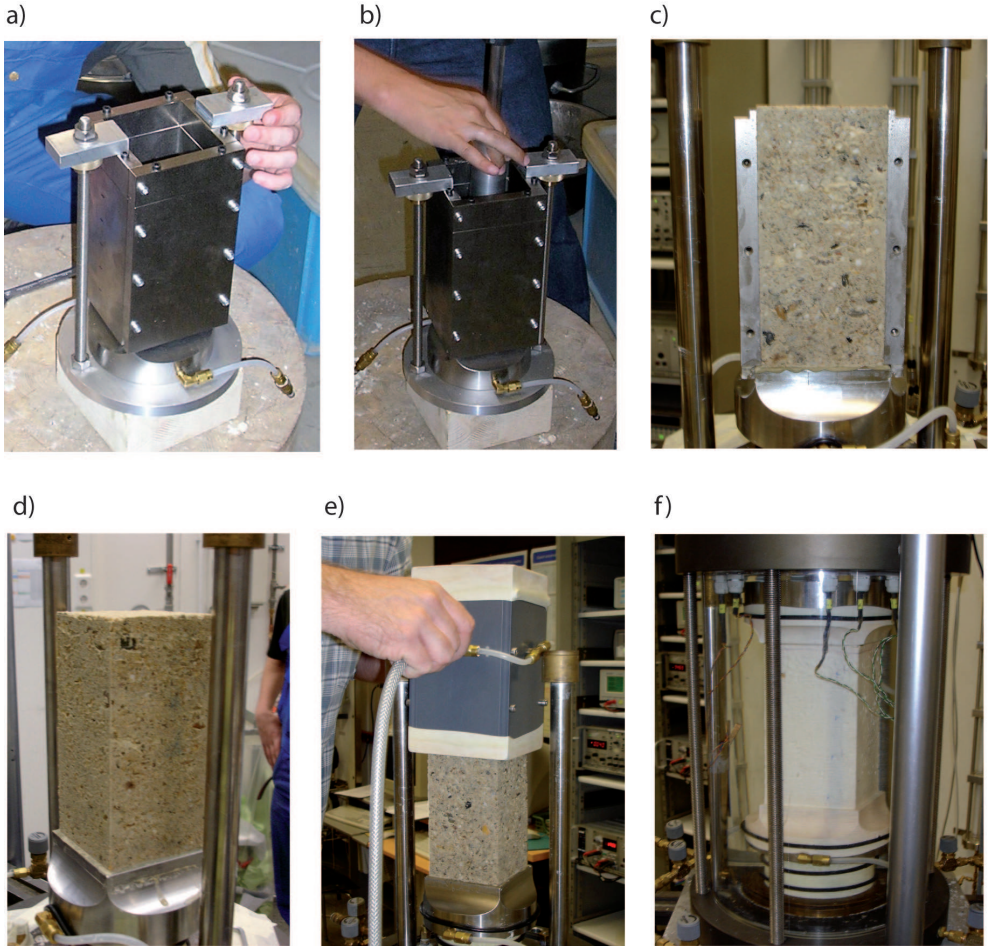

Figure 8: *Procedure for the preparation of an UGM specimen for triaxial tests: a) Steel mould fixed to the bottom end plate of the triaxial cell (preparation outside device) b) Moist tamping of specimen with miniature proctor hammer c) Specimen after removal of one side of the mould d) Specimen after removal of all sides of the mould e) Placement of membrane with a special stretcher f) Specimen prior to shearing*

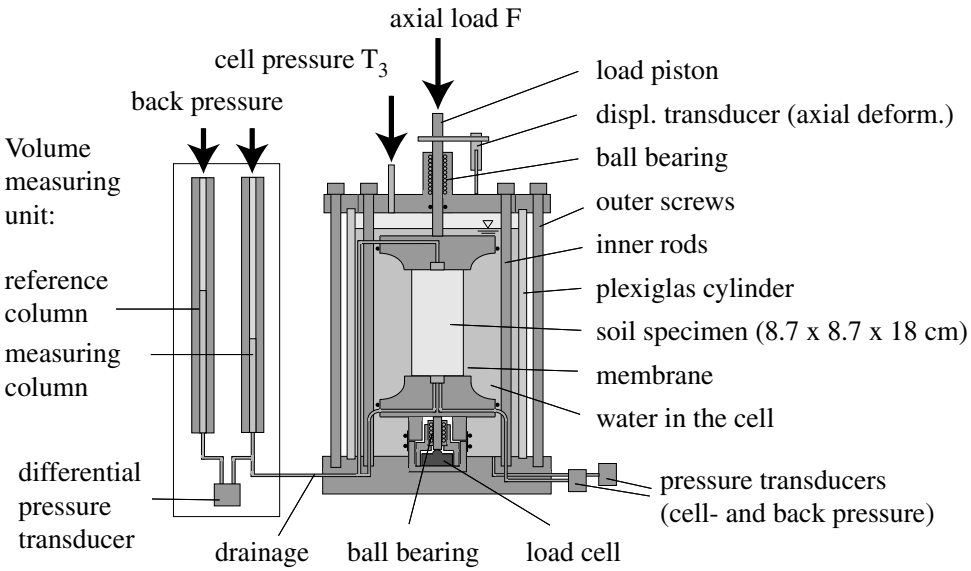

Figure 9: *Scheme of the used triaxial device*

expanded at the bottom. The observation may be explained by the fact that in comparison to the lower part of the sample, the upper part has experienced a lower number of blows during the preparation procedure.

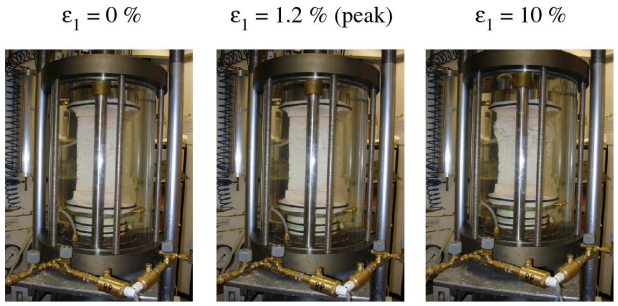

Figure 10: *Photos of an UGM specimen at different stages during a monotonic triaxial test*

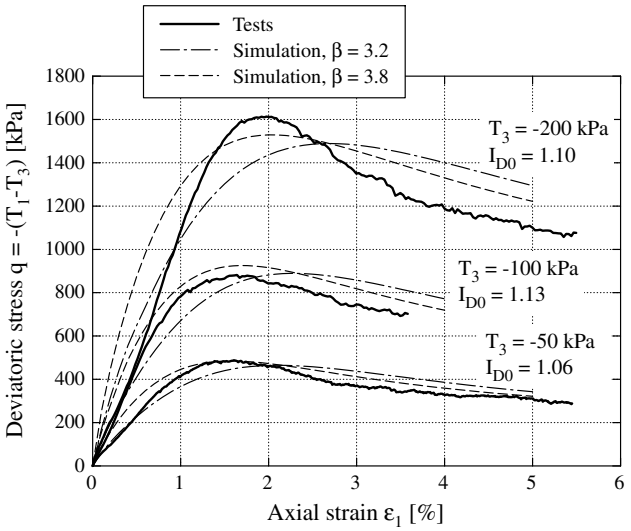

Figure 11: *q vs. ε_1 in monotonic triaxial tests with different confining pressures (experiment and simulation)*

The curves of deviatoric stress q and volumetric strain ε_v versus axial strain ε_1 are presented in Figs. 11 and 12. In Fig. 13 the peak stresses are shown in the p-q-plane. The well known decrease of the peak stress ratio $\eta_P = q_P/p_P$ with increasing lateral effective stress $-T_3$ would be even more pronounced if Test No. 1 would have been performed with a slightly higher initial density (similar to the values in the two other tests).

The constant α was determined from Eq. (19). The triples (η_P, p_P, e_P) from the three tests and the resulting values α are summarized in Table 2. The mean value $\alpha = 0.14$ has been obtained and further used.

It was interesting to know, if the specimen preparation method with the miniature proctor hammer or the high axial stresses during the tests affect the grain

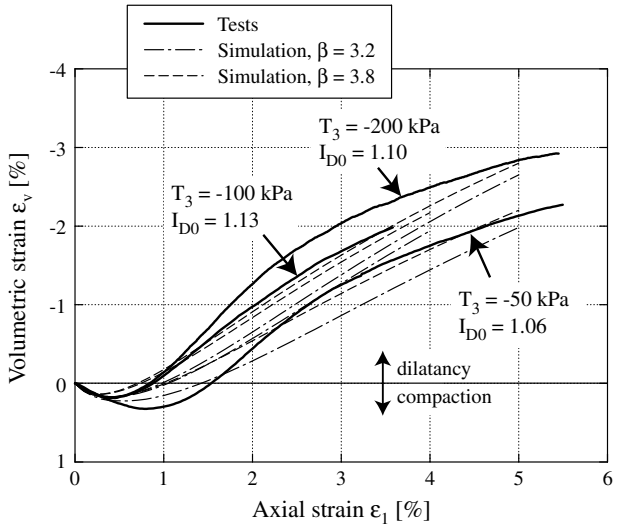

Figure 12: *ε_v vs. ε_1 in monotonic triaxial tests with different confining pressures (experiment and simulation)*

size distribution curve, i.e. if particle crushing takes place. A sieving was conducted after each monotonic triaxial test. In Fig. 1 the curves obtained after the tests are compared to the original one. A slight movement of the curves to the left, i.e. to smaller grain sizes was detected. The shift was observed to be larger with increasing lateral stress of the test. This could give hints for particle crushing, which is partly caused during specimen preparation and partly during a test.

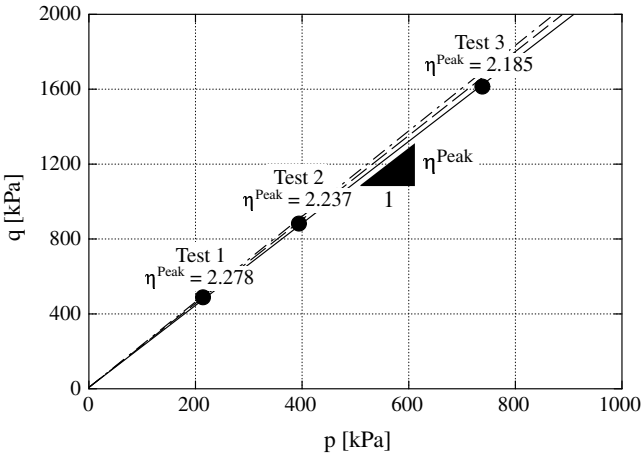

Figure 13: *Peak stresses in the p-q-plane*

The constant β was obtained from Eq. (21), i.e. from a comparison of the oedometric moduli for two different initial densities. The tests on loose UGM material (I_{D0} = 0.01 - 0.10) were supplemented by three tests on medium dense specimens (I_{D0} = 0.52 - 0.58). These tests were also performed on dry specimens. The UGM material was placed by pouring

Test No.	T_3 [kPa]	$I_{D,\mathrm{prep}}$ [-]	I_{D0} [-]	ϱ_d/ϱ_{Pr} [%]	q_{Peak} [kPa]	p_{Peak} [kPa]	η_{Peak} [-]	Y_{Peak} [-]	e_{Peak} [-]	φ_{Peak} [°]	α [-]
1	-50	1.06	1.06	95.1	487.9	214.2	2.278	1.174	0.221	55.6	0.147
2	-100	1.13	1.14	96.3	881.9	394.3	2.237	1.167	0.203	54.5	0.123
3	-200	1.10	1.11	95.8	1613.3	738.4	2.185	1.158	0.205	53.2	0.149
Mean		1.10	1.10				2.23		0.210	54.4	0.14

Table 2: Summary of constants α determined from three monotonic triaxial compression tests ($I_{D,\mathrm{prep}}$ = relative density after preparation, I_{D0} = relative density after consolidation)

φ_c [°]	h_s [MPa]	n [-]	e_{d0} [-]	e_{c0} [-]	e_{i0} [-]	α [-]	β [-]
38	97	0.24	0.225	0.444	0.511	0.14	3.2

Table 3: Hypoplastic constants of the tested UGM

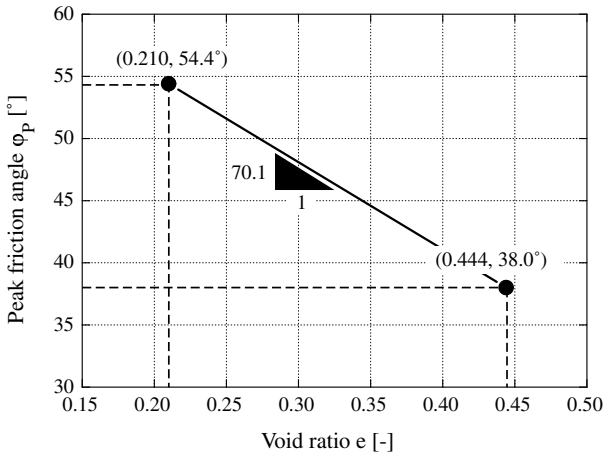

Figure 14: *Approximation of peak friction angle used for the analysis of the oedometric compression tests on medium dense specimens (determination of constant β)*

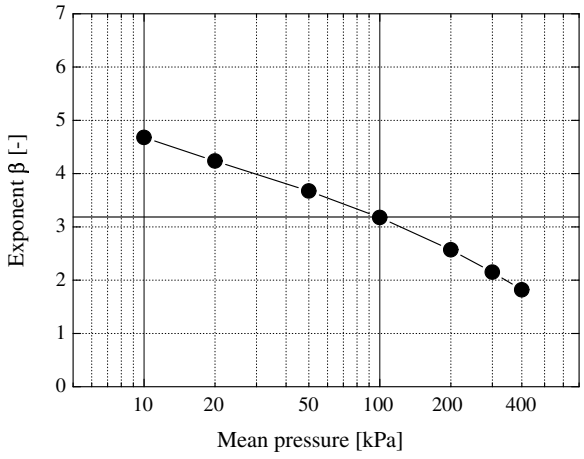

Figure 15: *Exponent β evaluated for different mean pressures p*

with a spoon and afterwards compacted by vibration (lateral hits to the oedometer chamber with a rubber hammer). The measured curves $e(p)$ are given in Fig. 7 (lower three curves). For the tests with I_{D0} = 0.52 - 0.58 the lateral stress was calculated using $K_0 = 1-\sin(\varphi_P)$ with the peak friction angle estimated from $\varphi_P = 54.4° - 70.1°(e - 0.210)$. This equation was derived from the knowledge of the critical friction angle $\varphi_c = 38.0°$ at $e \approx e_{\max} = 0.444$ and the peak friction angle $\varphi_P = 54.4°$ at $e_P = 0.210$ (mean value from the triaxial tests) and is illustrated in Fig. 14.

The constant β was evaluated for different mean pressures p. Fig. 15 reveals a significant decrease of β with p (a problem already detected also for other sands). Thus, it is not clear, which value of β should be chosen. A value $\beta = 3.2$ at $p = 100$ kPa was selected. In comparison to most values documented in the literature (see Appendix) this β-value is large. However, Herle [17] and Schünemann [39] report on similar values for limestone rockfill and ballast, respectively.

Finally, the eight hypoplastic constants are summarized in Table 3.

6 Re-calculation of element tests (numerical simulations)

The oedometric and triaxial tests were re-calculated with an element test program in which the hypoplastic model in the version proposed by von Wolffersdorff is implemented. The curves $e(p)$, $q(\varepsilon_1)$ and $\varepsilon_v(\varepsilon_1)$ of the simulations are added to Figs. 7, 11 and 12. In the case of the oedometric tests calculations are shown for the two initial void ratios $e_0 = 0.44$ and 0.33. The curves calculated with $\beta = 3.2$ were supplemented by those with $\beta = 3.8$ since this constant was found to

predict better the position of the peaks in the triaxial tests. However, as expected the re-calculation of the oedometric compression tests on the medium dense specimens look worse with $\beta = 3.8$ than with $\beta = 3.2$. In general, the agreement of the curves predicted by hypoplasticity and the experimental data is quite satisfactory.

7 Summary, conclusions and outlook

The determination of the material constants of the Wolffersdorff hypoplastic model [41] for an unbound granular material (UGM, mean grain size $d_{50} = 6.3$ mm, coefficient of uniformity $C_u = 100$) as used for base and subbase layers of flexible pavements is presented. Up to the present work, a set of hypoplastic material constants for an UGM was not documented in the literature. It is demonstrated that correlations of the constants with the granulometric properties (d_{50}, C_u) established for sand with 0.16 mm $\leq d_{50} \leq$ 2.0 mm and $1.4 \leq C_u \leq 7.2$ cannot be extrapolated for such well-graded materials. In order to determine a set of material constants for an UGM the procedure proposed by Herle [16] was applied. The triaxial tests were performed with specimens with a square cross-section. In a preliminary test series it was found that cylindrical and prismatic specimens deliver similar test results. In re-calculations of oedometric and triaxial tests a good prediction of the hypoplastic model could be demonstrated.

The further research will concentrate on permanent deformations of UGMs under cyclic loading. The results of cyclic triaxial tests with constant and variable confining pressure will be presented in a future publication together with possible constitutive descriptions.

8 Acknowledgments

The experimental work was done at the Institute of Soil Mechanics and Foundation Engineering at Ruhr-University Bochum. The stay of H. Rondón in Bochum was financed by scholarships of Colciencias and DAAD which is gratefully acknowledged herewith. Furthermore, the authors want to thank the laboratory assistants M. Skubisch and B. Kaminski for carefully performing the experiments.

References

[1] COST 337. Unbound Granular Materials for Road Pavements, Final Report of the Action. Luxembourg: Office for Official Publications of the European Communities. , 2000.

[2] Asphalt Institute (AI). Research and Development of the Asphalt Institute's Thickness Design Manual MS - 1, 9th Ed., College Park, Md. , 1982.

[3] L.Q. Anh Dan, F. Tatsuoka, and J. Koseki. Viscous shear stress-strain characteristics of dense gravel in triaxial compression. *Geotechnical Testing Journal, ASTM*, 2003.

[4] AUSTROADS. Pavement Design - A Guide to the Structural Design of Road Pavement, Sydney - Australia. , 1992.

[5] R. D. Barksdale and S. Y. Itani. Influence of Aggregate Shape on Base Behaviour. *Transportation Research Record*, (1227):173 – 182, 1989.

[6] E. Bauer. Calibration of a comprehensive constitutive equation for granular materials. *Soils and Foundations*, 36:13–26, 1996.

[7] A.W. Bishop and G.E. Green. The influence of end restraint on the compression strength of a cohesionless soil. *Géotechnique*, 15(3):243–266, 1965.

[8] M. Bühler. Experimental and numerical investigation of soil-foundation-structure interaction during monotonic, alternating and dynamic loading. Dissertation, Veröffentlichungen des Instituts für Bodenmechanik und Felsmechanik, Universität Karlsruhe, Heft 166, 2006.

[9] Shell International Petroleum Company. Shell Pavement Design Manual - Asphalt Pavement and Overlays for Road Traffic, London. , 1978.

[10] R. Cudmani. Modelación numérica de estructuras geotécnicas y taludes durante terremotos de gran magnitud. In *X Congreso y V Seminario Colombianos de Geotecnia*, 2004.

[11] R.O. Cudmani. Statische, alternierende und dynamische Penetration in nichtbindige Böden. Dissertation, Veröffentlichungen des Institutes für Bodenmechanik und Felsmechanik der Universität Fridericiana in Karlsruhe, Heft 152, 2001.

[12] A. R Dawson, M J Mundy, and M. Huhtala. European Research into Granular Material for Pavement Bases and Subbases. *Transportation Research Record*, pages 91–99, 2000.

[13] INVIAS Instituto Nacional de Vías. Especificaciones generales de construcción de carreteras. Bogotá D.C., Colombia, 2002.

[14] S. Goto, F. Tatsuoka, S. Shibuya, Y.-S. Kim, and T. Sato. A simple gauge for local small strain measurements in the laboratory. *Soils and Foundations*, 31(1):169–180, 1991.

[15] K. Hayano, M. Matsumoto, F. Tatsuoka, and J. Koseki. Evaluation of time-dependent deformation properties of sedimentary soft rock and their constitutive modeling. *Soils and Foundations*, 41(2):21–38, 2001.

[16] I. Herle. Hypoplastizität und Granulometrie einfacher Korngerüste. Promotion, Institut für Bodenmechanik und Felsmechanik der Universität Fridericiana in Karlsruhe, Heft Nr. 142, 1997.

[17] I. Herle. Granulometric Limits of Hypoplastic Models. *Institute of Theoretical and Applied Mechanics, Czech Academy of Sciences, Proseck, Task Quarterly, Scientific Bulletin of Academic Computer Centre in Gdansk*, 4(3):389–408, 2000.

[18] I. Herle and G. Gudehus. Determination of Parameters of a Hypoplastic Constitutive Model from Properties of Grain Assemblies. *Mechanics of Cohesive-Frictional Materials*, 4(5):461–486, 1999.

[19] HMSO. Design Manual for Roads and Bridges. Vol 7, HD 25/94, part 2, Foundations, 1994.

[20] E. Hoque, T. Sato, and F. Tatsuoka. Performance evaluation of LDTs for use in triaxial tests. *Geotechnical Testing Journal, ASTM*, 20(2):149–167, 1997.

[21] IDU. Instituto de Desarrollo Urbano and Universidad de Los Andes, Manual de Diseno de Pavimentos para Bogotá. Bogotá D.C., Colombia. , 2002.

[22] G.-L. Jiang, F. Tatsuoka, A. Flora, and J. Koseki. Inherent and stress-state-induced anisotropy in very small strain stiffness of a sandy gravel. *Géotechnique*, 47(3):509–521, 1997.

[23] D. Kolymbas. An outline of hypoplasticity. *Archive of Applied Mechanics*, 61:143–151, 1991.

[24] L. Kongsukprasert, R. Kuwano, and F. Tatsuoka. Effects of ageing with shear stress on the stress-strain behaviour of cement-mixed sand. In Tatsuoka et al., editor, *Advanced laboratory stress-strain testing of geomaterials*, pages 251–258. Balkema, 2001.

[25] TRL Transport Research Laboratory. A Guide to the Structural Design of Bitumen-Surfaced Roads in Tropical and Sub-tropical Countries. RN31, Draft 4th edition. , 1993.

[26] F. Lekarp, U. Isacsson, and A. Dawson. State of the art. II: Permanent strain response of unbound aggregates. *Journal of Transportation Engineering*, 126(1):76–83, 2000.

[27] A. B. Libreros Bertini. Hypo- und viskohypoplastische Modellierung von Kriech- und Rutschbewegungen, besonders infolge Starkbeben. Dissertation, Veröffentlichungen des Instituts für Bodenmechanik und Felsmechanik, Universität Karlsruhe, Heft 165, 2006.

[28] H. Matsuoka and T. Nakai. A new failure for soils in three-dimensional stresses. In *Deformation and Failure of Granular Materials*, pages 253–263, 1982. Proc. IUTAM Symp. in Delft.

[29] J. R. Morgan. The Response of Granular Materials to Repeated Loading. In *Proc., 3rd Conf., ARRB*, 1966.

[30] H. Nawir, F. Tatsuoka, and R. Kuwano. Experimental evaluation of the viscous properties of sand in shear. *Soils and Foundations*, 43(6):13–32, 2003.

[31] P.G. Nicholson, R.B. Seed, and H.A. Anwar. Elimination of membrane compliance in undrained triaxial testing. I. Measurement and evaluation. *Canadian Geotechnical Journal*, 30:727–738, 1993.

[32] A. Niemunis. Akkumulation der Verformung infolge zyklischer Belastung - numerische Strategien. In *Beiträge zum Workshop: Boden unter fast zyklischer Belastung: Erfahrungen und Forschungsergebnisse, Veröffentlichungen des Institutes für Grundbau und Bodenmechanik, Ruhr-Universität Bochum, Heft Nr. 32*, pages 1–20, 2000.

[33] A. Niemunis. Extended hypoplastic models for soils. Habilitation, Veröffentlichungen des Institutes für Grundbau und Bodenmechanik, Ruhr-Universität Bochum, Heft Nr. 34, 2003. available from `www.pg.gda.pl/~aniem/an-liter.html`.

[34] A. Niemunis and I. Herle. Hypoplastic model for cohesionless soils with elastic strain range. *Mechanics of Cohesive-Frictional Materials*, 2:279–299, 1997.

[35] A. Niemunis, T. Wichtmann, and T. Triantafyllidis. A high-cycle accumulation model for sand. *Computers and Geotechnics*, 32(4):245–263, 2005.

[36] American Association of State Highway and Transportation Officials (AASHTO). Guide for Design of Pavement Structures, Washington, D. C. , 1986.

[37] American Association of State Highway and Transportation Officials (AASHTO). Guide for Design of Pavement Structures, Washington, D. C. , 1993.

[38] H. A. Rondón and A. Lizcano. Modelos de comportamiento de materiales granulares para pavimentos y aplicación de la ley constitutiva hipoplástica. In *III Jornadas Internacionales de Ingeniera Civil. Cuba*, 2006.

[39] A Schünemann. Numerische Modelle zur Beschreibung des Langzeitverhaltens von Eisenbahnschotter unter alternierender Beanspruchung. Dissertation, Veröffentlichungen des Instituts für Bodenmechanik und Felsmechanik, Universität Karlsruhe, Heft 168, 2006.

[40] G.T.H. Sweere. *Unbound granular bases for roads*. PhD thesis, Delft University of Technology, Netherlands, 1990.

[41] P.-A. von Wolffersdorff. A hypoplastic relation for granular materials with a predefined limit state surface. *Mechanics of Cohesive-Frictional Materials*, 1:251–271, 1996.

[42] W. C. S. Wehr. Granulatumhllte Anker und Ngel - Sandanker. Dissertation, Veröffentlichungen des Instituts für Bodenmechanik und Felsmechanik, Universität Karlsruhe, Heft 146, 1999.

[43] S. Werkmeister, A. Dawson, and F. Wellner. Permanent Deformation Behaviour of Granular Materials and the Shakedown Concept. *Transportation Research Record*, (1757):75 – 81, 2001.

[44] S. Werkmeister, A. Dawson, and F. Wellner. Pavement Design Model of Unbound Granular Materials. *Journal of Transportation Engineering*, 130:665 – 674, 2004.

[45] T. Wichtmann. Explicit accumulation model for non-cohesive soils under cyclic loading. Dissertation, Schriftenreihe des Institutes für Grundbau und Bodenmechanik der Ruhr-Universität Bochum, Heft 38, available from www.rz.uni-karlsruhe.de/∼gn97/, 2005.

Appendix B: Summary of hypoplastic constants for various materials

Material	Grain shape	d_{50}	C_u	ϱ_s	φ_c	h_s	n	e_{d0}	e_{c0}	e_{i0}	α	β	Ref.
		[mm]	[-]	[g/cm^3]	[°]	[MPa]	[-]	[-]	[-]	[-]	[-]	[-]	[-]
Sandy fill				2.65	32.1	4000	0.25	0.55	0.95	1.05	0.07	1.00	[8]
Silty Sand I (S)				2.65	32.9	750	0.45	0.831	1.281	1.41	0.05	1.00	
Silty Sand II (S)				2.65	37.2	1200	0.27	0.53	0.864	0.996	0.127	1.05	
Stuttgart (S)				2.65	33.0	2600	0.30	0.60	0.98	1.15	0.10	1.00	
Quartz (S)		0.25	2.35		33.0	2600	0.30	0.60	0.98	1.15	0.10	1.00	[10]
Tierra Blanca					36.0	100	0.10	0.90	1.40	1.60	0.08	1.00	
Ticino (S)	compact	0.53	1.60	2.67	31.0	250	0.68	0.59	0.94	1.11	0.11	1.00	[11]
Toyoura (S)	subrounded	0.21	1.30	2.65	32.0	120	0.69	0.61	0.98	1.13	0.12	1.00	
L. Buzzard (S)	compact	0.85	1.30	2.65	31.0	6400	0.45	0.49	0.79	0.94	0.16	1.00	
Hokksund (S)	subround. - ang.	0.43	2.20	2.70	31.0	150	0.70	0.53	0.87	1.01	0.09	1.00	
Monterey (S)	subround.	0.37	1.60	2.65	32.0	8000	0.35	0.54	0.83	0.90	0.07	1.00	
Quiou (S)	subround. - ang.	0.50	3.50	2.66	36.0	75	0.45	0.831	1.281	1.41	0.05	1.00	
Dogs Bay (S)	subround. - ang.	0.25	2.66	2.75	40.3	30	0.72	0.981	1.827	2.192	0.05	1.00	
Kleinkoschen (S)	subround. - ang.	0.50	3.10	2.64	34.0	7450	0.11	0.45	0.90	1.04	0.14	1.00	
Zwenkau B (S)		0.4-0.75	7-12	2.63	32.0	42	0.22	0.60	1.14	1.31	0.10	3.00	
Zwenkau C (S)		0.2-0.75	50-22	2.43	30.0	10	0.26	0.73	1.28	1.48	0.14	1.50	
Zwenkau D (S)		0.15-0.35	12-4.5	2.65	30.0	80	0.24	0.61	1.10	1.27	0.10	2.40	
Erksak (S)	subround.	0.355	2.20	2.65	30.0	80	0.65	0.525	0.85	1.00	0.11	1.00	
Mai-Liao (S)	subround. - ang.	0.12	2.50	2.69	31.5	32	0.324	0.57	1.04	1.20	0.40	1.00	
Toyoura (S)	ang./subrounded	0.16	1.46	2.64	30.0	2600	0.27	0.61	0.98	1.10	0.18	1.00	[16]
Hochstetten (S)	subrounded	0.20	1.60	2.65	33.0	1500	0.28	0.55	0.95	1.05	0.25	1.50	
Schlabendorf (S)	subrounded	0.25	3.09	2.65	33.0	1600	0.19	0.44	0.85	1.00	0.25	1.00	
Hostun (S)	ang./subrounded	0.35	1.68	2.67	31.0	1000	0.29	0.61	0.91	1.09	0.13	2.00	
Karlsruhe (S)	subrounded	0.40	1.85	2.65	30.0	5800	0.28	0.53	0.84	1.00	0.13	1.05	
Zbraslav (S)	ang./subrounded	0.50	2.62	2.65	31.0	5700	0.25	0.52	0.82	0.95	0.13	1.00	
Ottawa (S)	round.-subround.	0.53	1.70	2.66	30.0	4900	0.29	0.49	0.76	0.88	0.10	1.00	
Ticino (S)	ang./subround.	0.55	1.40	2.68	31.0	5800	0.31	0.60	0.93	1.05	0.20	1.00	
Silver Leighton Buzzard (S)	subround.	0.62	1.11	2.66	30.0	8900	0.33	0.49	0.79	0.90	0.14	1.00	
Hochstetten (G)	subrounded	2.00	7.20	2.65	36.0	32000	0.18	0.26	0.45	0.50	0.10	1.80	
Kunststoff	subrounded	3.00	1.00	1.07	32.0	110	0.33	0.53	0.73	0.80	0.08	1.00	
Weizen	subrounded	3.70	1.00	1.25	39.0	20	0.37	0.57	0.84	0.95	0.02	1.00	
Lausitz (S)	subrounded	0.25	3.09	2.65	33.0	1600	0.19	0.44	0.85	1.00	0.25	1.00	[18]
Sedlec (L)		0.02	150	2.70	30.0	0.79	0.126	0.73	1.37	1.58	0.15	1.00	[17]
Limestone (RF)	subrounded		20	2.72	38.0	10	0.36	0.31	0.68	0.78	0.10	3.10	
Hochstetten (S)					33.0	1000	0.25	0.55	0.95	1.05	0.25	1.50	[27]
Colentina (G)					36.0	170	0.225	0.62	0.99	1.13	0.10	1.00	
Mostistea (S)					36.0	320	0.28	0.26	0.45	0.50	0.10	1.80	
Eisenbahnschotter (B)					50.0	150	0.40	0.65	1.00	1.15	0.05	4.00	[39]
Sand 1 (S)	subangular	0.55	1.80	2.65	31.2	591	0.50	0.577	0.874	1.005	0.12	1.00	[45]
ZFS (S)	subangular	0.21	2.00	2.66	32.8	5580	0.30	0.575	0.908	1.044	0.12	1.60	
Stuttgart (G)		2.80			37.0	190	0.52	0.58	0.88	1.06	0.25	1.50	[42]
Kelsterbach (S)		0.90			33.0	290	0.42	0.52	0.82	1.00	0.25	1.10	
Granular material I (S)		1.60			34.0	332	0.47	0.625	0.862	0.991	0.25	1.50	
Granular mat. II (G)		4.00			38.0	58	0.70	0.655	0.823	0.946	0.25	1.10	

Table 4: B = ballast; G = gravel; L = loess; RF = rockfill; S = sand.